Available online at www.sciencedirect.com
ScienceDirect
Journal of the European Ceramic Society 31 (2011) 3073–3079
www.elsevier.com/locate/jeurceramsoc

Effect of double doping on crystal structure and electrical conductivity of CaO and WO_3-doped Bi_2O_3

Cheng-Yen Hsieh, Hao-Sheng Wang, Kuan-Zong Fung *

Department of Materials Science and Engineering, National Cheng Kung University, Tainan 701, Taiwan, ROC

Available online 8 May 2011

Abstract

The atomic arrangement of WO_3-doped Bi_2O_3 was found similar to that of the fluorite structure. However, the electrical conductivity of WO_3-doped Bi_2O_3 is significantly lower than that of commonly used Y_2O_3-doped Bi_2O_3. The structure and electrical conductivity of samples formulated as $(Ca_xW_{0.15}Bi_{0.85-x})_2O_{3.45-x}$ ($x = 0$, 0.1, 0.2 and 0.3) were investigated. The as-sintered $(W_{0.15}Bi_{0.85})_2O_{3.45}$ and $(Ca_{0.1}W_{0.15}Bi_{0.75})_2O_{3.35}$ exhibit similar single tetragonal structure that is isostructural with $7Bi_2O_3{\cdot}2WO_3$. Therefore, $(W_{0.15}Bi_{0.85})_2O_{3.45}$ and $(Ca_{0.1}W_{0.15}Bi_{0.75})_2O_{3.35}$ formed a superstructure consisting of 10 enlarged cubic fluorite subcells. However, the as-sintered samples consist of a tetragonal structure and tetragonal $CaWO_4$ for $x = 0.2$ and 0.3 because the oxygen vacancy concentration increases. The conductivities of $(Ca_xW_{0.15}Bi_{0.85-x})_2O_{3.45-x}$ ($x = 0$, 0.1, 0.2 and 0.3) did not exhibit linear dependence with x value. The best conductivity is 2.35×10^{-2} S cm^{-1} at 700 °C for $x = 0.1$ that is higher than that of Ca-free $(W_{0.15}Bi_{0.85})_2O_{3.45}$. The higher conductivity of $(Ca_{0.1}W_{0.15}Bi_{0.75})_2O_{3.35}$ than $(W_{0.15}Bi_{0.85})_2O_{3.45}$ may result from the higher anion vacancy concentration and more symmetrical structure.

Keywords: Electrolyte; Electrical conductivity; Fluorite structure; Bismuth oxide

1. Introduction

Yttria-stabilized zirconia (YSZ) electrolytes are widely for solid electrochemical devices, especially solid oxide fuel cell (SOFC). However, YSZ must be operated at above 800 °C in order to gain high enough ionic conductivity.[1] Such high operating temperature limited many potential applications. Therefore, it is necessary to reduce the operating temperature and to search an oxygen ionic conductor with high ionic conductivity at intermediate temperatures (≤800 °C). Up to date, one oxygen ionic conductor cubic δ-Bi_2O_3 with highest ionic conductivity at the temperature ≥723 °C is reported.[2] For many solid state electrolytes based on Bi_2O_3 are destabilized to hold the fluorite structure at lower temperature range.[2–12] One interesting case, WO_3-doped Bi_2O_3, was found to exhibit stable fluorite-based structures to room temperature and high ion conductivity.[4,6] When the amount of WO_3 added in the range between 11.9 and 15.15 mol%, the WO_3-doped Bi_2O_3 exhibits a tetragonal structure, i.e., $7Bi_2O_3{\cdot}2WO_3$ which shows subcells similar to that of CaF_2 fluorite structure. But the Bi and W ions do not randomly arrange in $7Bi_2O_3{\cdot}2WO_3$ unit cells.

The relationship between unit cell of tetragonal $7Bi_2O_3{\cdot}2WO_3$ and that of cubic fluorite δ-Bi_2O_3 is $a_t = 2a_f + b_f$, $b_t = -a_f + 2b_f$, and $c_t = 2c_f$.[13–16] a_t, b_t, c_t represent lattice vectors of tetragonal $7Bi_2O_3{\cdot}2WO_3$, and a_f, b_f, c_f represent lattice vectors of cubic fluorite δ-Bi_2O_3. Recently, Abrahams et al.[17,18] investigated Bi_2O_3–WO_3–Nb_2O_5 and Bi_2O_3–Y_2O_3–Nb_2O_5. Some compositions show a defect fluorite-type structure. According to the reports by Abrahams et al., the addition of appropriate dopant is capable of eliminating the order arrangement of $7Bi_2O_3{\cdot}2WO_3$ unitcell. Y_2O_3 was found to be an appropriate dopant to stabilize cubic fluorite structure in $(YO_{1.5})_x(WO_3)_{0.15}(BiO_{1.5})_{0.85-x}$ solid solution due to the decrease of mismatch in size and valence between Bi^{3+} and W^{6+}.[19]

The ionic radius of Ca^{2+}, 1.12 Å is similar to that of Y^{3+}, 1.109 Å.[20] Addition of CaO in $(CaO)_x(WO_3)_{0.15}(BiO_{1.5})_{0.85-x}$ may be appropriate compositions to stabilize cubic fluorite structure and enhance the oxygen conductivity further by the increase of the oxygen vacancy concentration. Therefore, this study used CaO as dopant to stabilize cubic fluorite structure in $(CaO)_x(WO_3)_{0.15}(BiO_{1.5})_{0.85-x}$ solid solution. In this study, the

* Corresponding author. Tel.: +886 62757575x62969; fax: +886 62380208.
E-mail address: z8702009@email.ncku.edu.tw (K.-Z. Fung).

0955-2219/$ – see front matter © 2011 Elsevier Ltd. All rights reserved.
doi:10.1016/j.jeurceramsoc.2011.04.011

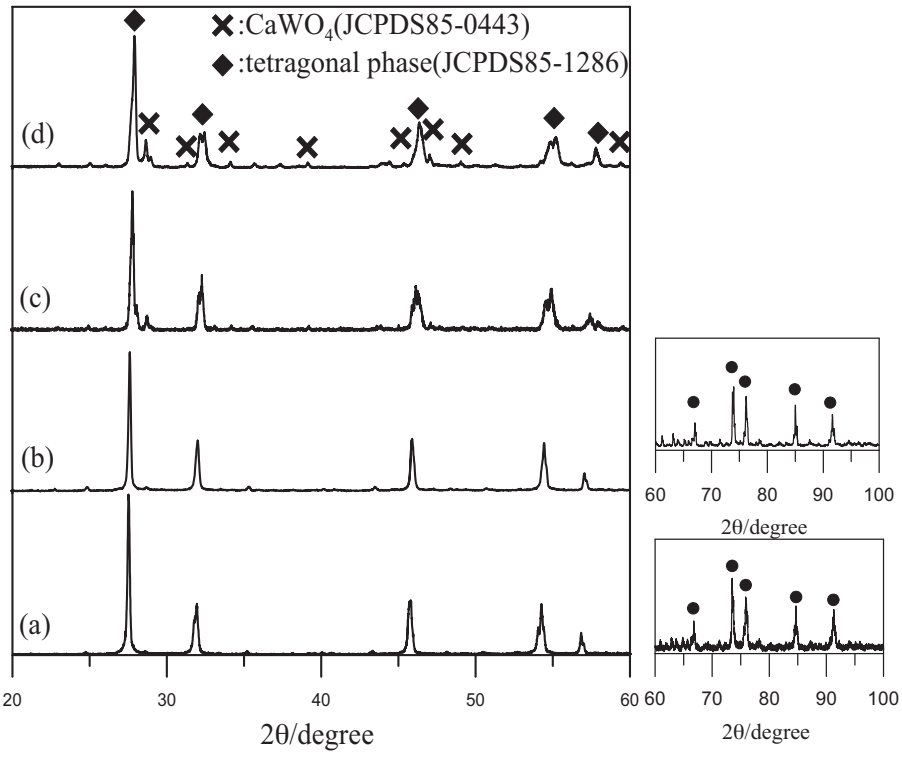

Fig. 1. XRD patterns of as-sintered $(CaO)_x(WO_3)_{0.15}(BiO_{1.5})_{0.85-x}$ for x = (a) 0, (b) 0.1, (c) 0.2, and (d) 0.3.

structures of $(CaO)_x(WO_3)_{0.15}(BiO_{1.5})_{0.85-x}$ (x = 0, 0.1, 0.2 and 0.3) are carefully examined by XRD, SEM and TEM. The oxygen conductivity was measured using AC Impedance technique in air at temperature ranging from 300 °C to 700 °C.

2. Experiment procedure

2.1. Sample preparation

The compositions of $(CaO)_x(WO_3)_{0.15}(BiO_{1.5})_{0.85-x}$ (x = 0, 0.1, 0.2 and 0.3) were synthesized in air by solid state reaction. The stoichiometric $CaCO_3$ (Showa, 99.9%) and WO_3 (Alfa, 99.8%) were mixed with Bi_2O_3 (Alfa, 99%). After ball-milling with ethanol for 24 h, the powder mixtures were dried and sieved through a 200-mesh screen. The mixed powders were calcined in air at 800 °C for 5 h. Subsequently, the powder was die-pressed into disks. After cold-isostatic pressing at 100 MPa, the disks were sintered in air between 800 and 1100 °C for 24 h. Then the disks were cooled to room temperature in furnace. The sintered samples were polished by aluminum oxide of grain size 1 and 0.3 μm, and followed by thermal etching between 800 and 1000 °C for 3 h.

Table 1
The lattice parameters and activation energies of $(CaO)_x(WO_3)_{0.15}(BiO_{1.5})_{0.85-x}$ (x = 0, 0.1, 0.2 and 0.3).

x	Lattice parameters (Å)	Activation energy (kJ/mol)
0	a = 12.52, c = 11.26	79
0.1	a = 12.47, c = 11.17	87
0.2	a = 12.38, c = 11.16	90
0.3	a = 12.30, c = 11.09	134

2.2. XRD, TEM and SEM analyses

The structure of $(Ca_xW_{0.15}Bi_{0.85-x})_2O_{3.45-x}$ (x = 0.1, 0.2 and 0.3) was examined by X-ray diffractometer (XRD), scanning and transmission electron microscope (TEM). The oxygen conductivity was measured using 2-probe technique in air at temperature ranging from 300 °C to 700 °C.

X-ray diffraction data were collected by Rigaku Multi-Flex X-ray diffractometer with graphite-monochromated Cu Kα radiation. To examine the structures and lattice parameters, respective samples were analyzed by XRD using a scanning rate of 1°/min at the 2θ range from 20° to 60° and operating at 30 kV, 20 mA. Further identification of the structure was by selected area electron diffraction (SAED). The electron microscope employed was FEI E.O Tecnai F20 G2 MAT S-TWIN Field Emission Gun Transmission Electron Microscope. To observe the morphological differences of the synthesized and annealed sample surfaces, the samples were examined using a field emission scanning electron microscopes (FESEM) (XL40 FEG PHILIPS) operating at 15 kV with carbon coating. The samples showing dual phases were analyzed by an energy dispersion X-ray spectrometer (EDAX XL-40135-10).

2.3. Conductivity measurement

Platinum electrodes were pasted on the polished surfaces of the sintered samples after drying at 800°C for 2 h. Subse-

quently, the samples were fixed between two Al_2O_3 fixtures, and Ag wires were used to connect Pt electrodes and the Solartron 1255B\1287. The oxygen conductivity was measured by AC Impedance technique in the frequency range 1 Hz to 10^6 Hz at temperature ranging from 300 °C to 700 °C.

3. Results and discussion

3.1. Structure characterization

3.1.1. $(CaO)_x(WO_3)_{0.15}(BiO_{1.5})_{0.85-x}$ for $x = 0$ and 0.1

Fig. 1 shows the XRD patterns of as-sintered $(CaO)_x(WO_3)_{0.15}(BiO_{1.5})_{0.85-x}$ for x = 0–0.3. The sintering temperatures of $(CaO)_x(WO_3)_{0.15}(BiO_{1.5})_{0.85-x}$ increase with adding CaO and are 800 °C, 900 °C, 1000 °C, 1100 °C for x = 0, 0.1, 0.2, 0.3, respectively. The samples formulated as $(W_{0.15}Bi_{0.85})_2O_{3.45}$ and $(Ca_{0.1}W_{0.15}Bi_{0.75})_2O_{3.35}$ exhibit similar XRD patterns which are similar to cubic fluorite structure. However, the enlarged XRD patterns ranging from 60° to 100° show obviously splitting peaks. Therefore, the as-sintered $(W_{0.15}Bi_{0.85})_2O_{3.45}$ and $(Ca_{0.1}W_{0.15}Bi_{0.75})_2O_{3.35}$ exhibit a single tetragonal structure that is isostructural with $7Bi_2O_3{\cdot}2WO_3$.[13] The lattice parameters of $(W_{0.15}Bi_{0.85})_2O_{3.45}$ and $(Ca_{0.1}W_{0.15}Bi_{0.75})_2O_{3.35}$ are shown in Table 1 which are about $\sqrt{5}$ and 2 times that of δ-Bi_2O_3 (5.66 Å). Therefore, $(W_{0.15}Bi_{0.85})_2O_{3.45}$ and $(Ca_{0.1}W_{0.15}Bi_{0.75})_2O_{3.3}$ formed a superstructure consisting of 10 enlarged cubic fluorite subcells.

Zhou[14] also showed XRD pattern of $7Bi_2O_3{\cdot}2WO_3$ was similar to cubic fluorite structure but SAED patterns of $7Bi_2O_3{\cdot}2WO_3$ showed additional diffraction spots to the tetragonal structure. The structure of as-sintered $(Ca_{0.1}W_{0.15}Bi_{0.75})_2O_{3.35}$ was further identified by TEM. Fig. 2 shows SAED patterns of as-sintered $(Ca_{0.1}W_{0.15}Bi_{0.75})_2O_{3.35}$ along [1 $\bar{3}$ 0] and [3 1 $\bar{5}$] which are very similar to those of $7Bi_2O_3{\cdot}2WO_3$.[14] SAED patterns of as-sintered $(Ca_{0.1}W_{0.15}Bi_{0.75})_2O_{3.35}$ reveal the superlattice derived from δ-Bi_2O_3. According to the diffraction spots of superlattice and cubic phase, the relationship of reciprocal lattices between the superlattice and cubic fluorite δ-Bi_2O_3 is expressed as Eq. (1).

$$\begin{bmatrix} \frac{2}{5} & \frac{1}{5} & 0 \\ \frac{\bar{1}}{5} & \frac{2}{5} & 0 \\ 0 & 0 & \frac{1}{2} \end{bmatrix} \begin{bmatrix} a*\mathrm{f} & b*\mathrm{f} & c*\mathrm{f} \end{bmatrix} = \begin{bmatrix} a*\mathrm{t} & b*\mathrm{t} & c*\mathrm{t} \end{bmatrix} \quad (1)$$

$a*\mathrm{f}$, $b*\mathrm{f}$, $c*\mathrm{f}$ represent reciprocal lattice vectors of cubic fluorite δ-Bi_2O_3, and $a*\mathrm{t}, b*\mathrm{t}, c*\mathrm{t}$ represent reciprocal lattice vectors of tetragonal $7Bi_2O_3{\cdot}2WO_3$. The relationship between the superlattice and cubic fluorite δ-Bi_2O_3 could be expressed as Eq. (2).

$$\begin{bmatrix} a\mathrm{f} & b\mathrm{f} & c\mathrm{f} \end{bmatrix} \begin{bmatrix} 2 & \bar{1} & 0 \\ 1 & 2 & 0 \\ 0 & 0 & 2 \end{bmatrix} = \begin{bmatrix} a\mathrm{t} & b\mathrm{t} & c\mathrm{t} \end{bmatrix} \quad (2)$$

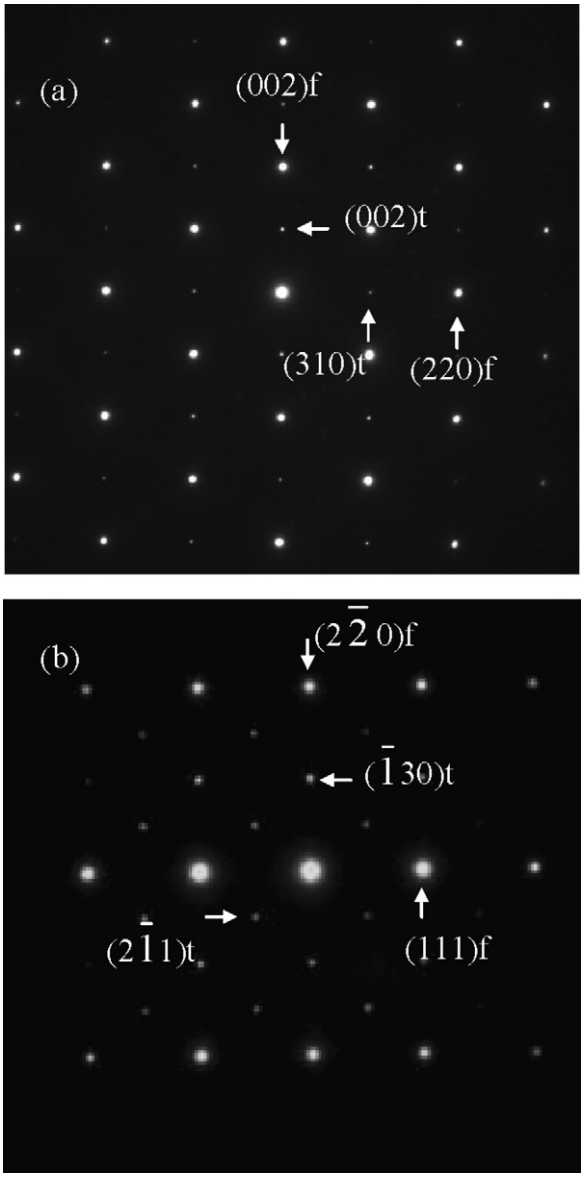

Fig. 2. SAED patterns of $(Ca_{0.1}W_{0.15}Bi_{0.75})_2O_{3.35}$ along (a) [1 $\bar{3}$ 0] and (b) [3 1 $\bar{5}$].

Therefore, the relationship between the superlattice and cubic fluorite δ-Bi_2O_3 is also $a_t = 2a_f + b_f$, $b_t = -a_f + 2b_f$ and $c_t = 2c_f$ which is the same as $7Bi_2O_3{\cdot}2WO_3$. From XRD and TEM results, $(W_{0.15}Bi_{0.85})_2O_{3.45}$ and $(Ca_{0.1}W_{0.15}Bi_{0.75})_2O_{3.35}$ exhibit similar tetragonal structure that is isostructural with $7Bi_2O_3{\cdot}2WO_3$. The atomic arrangement of superstructured $(WO_3)_{0.15}(BiO_{1.5})_{0.85}$ can be found in the author's previous work.[21] The formation of superstructure is caused by an ordered arrangement of W^{6+} and Bi^{3+} cations. The ionic radius of Bi^{3+}, 1.17 Å[20] is double larger than that of W^{6+}, 0.6 Å.[20] The ordered cation arrangement is simply due to the mismatch in ionic radius and valence. Although the substitution of Ca^{2+} (1.12 Å) for Bi^{3+} minimizes the mismatch in ionic radius, increases the mismatch in valence. Addition of CaO has no effect to stabilize the cubic fluorite structure in $(CaO)_x(WO_3)_{0.15}(BiO_{1.5})_{0.85-x}$ solid solution.

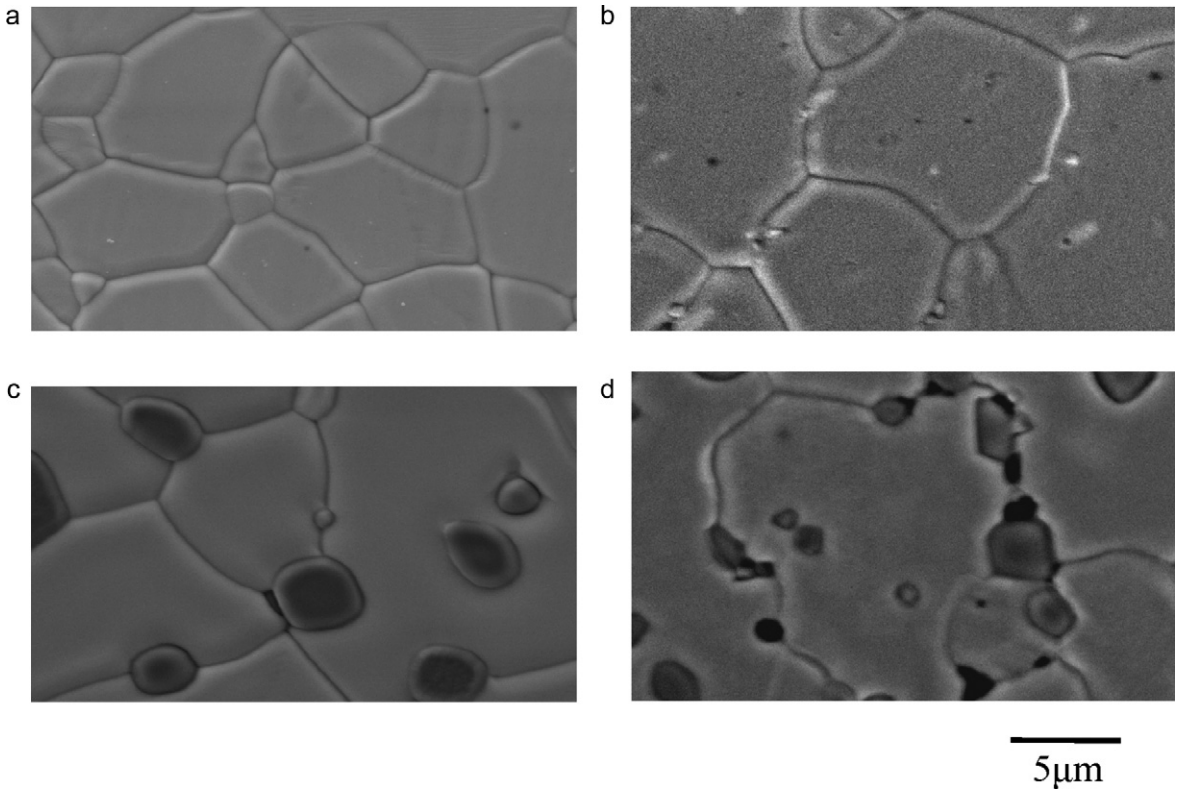

Fig. 3. SEM micrographs of thermal-etched $(Ca_xW_{0.15}Bi_{0.85-x})_2O_{3.45-x}$ for x = (a) 0, (b) 0.1, (c) 0.2 and (d) 0.3.

3.1.2. Formation of $CaWO_4$

In Fig. 1(c) and (d), the matrix is tetragonal structure and a second phase tetragonal $CaWO_4$ appears in the samples $(CaO)_x(WO_3)_{0.15}(BiO_{1.5})_{0.85-x}$ of $x = 0.2$ and 0.3. It is suggested that the solubility limit of CaO in $(CaO)_x(WO_3)_{0.15}(BiO_{1.5})_{0.85-x}$ was below 20 mol% and the excessive addition of CaO results in the formation of a second phase $CaWO_4$. The tetragonal structure of matrix is also isostructural with $7Bi_2O_3{\cdot}2WO_3$ and the composition of matrix is expected to change after $CaWO_4$ formation. In Fig. 1(c) and (d), the volume fraction of second phase $CaWO_4$, V_2, by XRD was estimated by integrated peak area of $CaWO_4$ and the tetragonal phase. The molar fraction, m, was estimated from the volume fraction by XRD as follow:

$$V_2 = \frac{I_2}{I_t + I_2} \tag{3}$$

$$m = \frac{V \times D}{M} \tag{4}$$

where I_2 and I_t denote the integrated peak area of $CaWO_4$ and the tetragonal phase, respectively. D and M denote the theoretical density and molecular weight, respectively. The theoretical density and molecular weight of $CaWO_4$ are 6.116 g/cm^3 and 287.93 g/mol. For the samples $(CaO)_x(WO_3)_{0.15}(BiO_{1.5})_{0.85-x}$ of $x = 0.2$ and 0.3, the measured densities by Archimedean method are 7.32, 6.72 g/cm^3 and the molecular weights are 394.828, 359.432 g/mol, respectively. From XRD patterns, the volume fractions of second phase $CaWO_4$ are estimated by integrated peak area showing 14 vol% and 26 vol% for the samples $(CaO)_x(WO_3)_{0.15}(BiO_{1.5})_{0.85-x}$ of $x = 0.2$ and 0.3. Therefore, the molar fractions of second phase $CaWO_4$ are 8.2% and 15% in these samples, respectively. Finally, the compositions of the tetragonal phases were estimated to be $(CaO)_{0.173}(WO_3)_{0.119}(BiO_{1.5})_{0.708}$ and $(CaO)_{0.265}(WO_3)_{0.088}(BiO_{1.5})_{0.647}$ for the samples $(CaO)_x(WO_3)_{0.15}(BiO_{1.5})_{0.85-x}$ of $x = 0.2$ and 0.3. Moreover, the compositions are constant to the results of EDX. According to the compositions, the oxygen vacancy concentrations of matrix increase as x increasing. The oxygen vacancies may result in strong repulsion from cation due to lack of screening effect,[22] so the cubic structure cannot be stabilized for $x = 0.2$ and 0.3.

3.1.3. SEM observation

The microstructures were further examined by SEM to verify the results of XRD. Fig. 3 shows SEM micrographs of thermally etched $(Ca_xW_{0.15}Bi_{0.85-x})_2O_{3.45-x}$ Fig. 3(a) and (b) shows an isotropic and single-phase microstructure. But the other types of the grains were clearly observed, as shown in Fig. 3(c) and (d). It is suggested that the samples $(CaO)_x(WO_3)_{0.15}(BiO_{1.5})_{0.85-x}$ $x = 0.2$, 0.3 composed of two phases. In Fig. 3(c) and (d), the dark grains have similar Ca and W contents but negligible Bi content based on EDX results. Therefore, it is suggested the composition of dark grains corresponds to the second phase, $CaWO_4$.

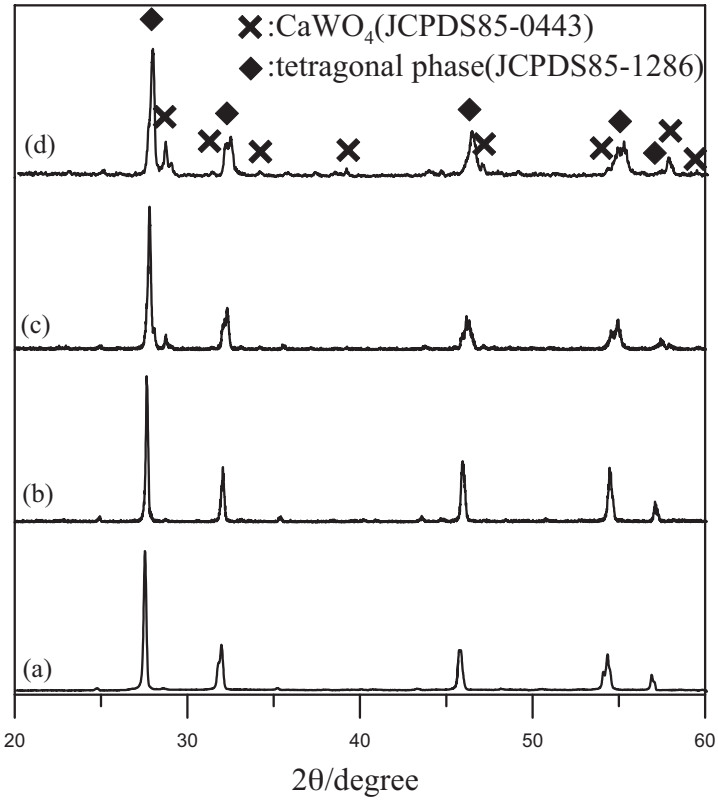

Fig. 4. XRD patterns of $(Ca_xW_{0.15}Bi_{0.85-x})_2O_{3.45-x}$ after annealing at 600 °C for 500 h. x = (a) 0, (b) 0.1, (c) 0.2 and (d) 0.3.

3.2. Thermal stability after heat treatment at 600 °C

As mentioned above, $(W_{0.15}Bi_{0.85})_2O_{3.45}$ and $(Ca_{0.1}W_{0.15}Bi_{0.75})_2O_{3.35}$ formed a superstructure consisting of 10 enlarged cubic fluorite subcells. The cubic yttria stabilized bismuth oxide is known as a metastable phase and may transform from cubic to rhombohedral phase after heat treatment at 600 °C.[8] Thus, the stabilization of as-sintered $(CaO)_x(WO_3)_{0.15}(BiO_{1.5})_{0.85-x}$ samples in this study was further examined by long time heat treatment. Fig. 4 shows XRD patterns of (Ca*x*W0.15Bi0.85−*x*)2O3.45−*x* after annealing at 600 °C for 500 h. The samples $(W_{0.15}Bi_{0.85})_2O_{3.45}$ and $(Ca_{0.1}W_{0.15}Bi_{0.75})_2O_{3.35}$ still exhibit a single tetragonal structure after annealing at 600 °C for 500 h. Fig. 4(c) and (d) that are similar to Fig. 1(c) and (d) shows the samples $(CaO)_x(WO_3)_{0.15}(BiO_{1.5})_{0.85-x}$ of $x = 0.2$ and 0.3 maintain the mixture of tetragonal phase and the second phase, $CaWO_4$. From these results, no similar cubic → rhombohedral phase transformation was observed for tetragonal matrix, so the tetragonal phase of the samples $(CaO)_x(WO_3)_{0.15}(BiO_{1.5})_{0.85-x}$ of $x = 0$, 0.1, 0.2 and 0.3 were stable after annealing at 600 °C for 500 h. The rhombohedral structures can be described as a regular repetition along the *c*-axis of identical fluorite-like sheets, and the oxygen vacancies are located in the intersheets that parallel to (1 1 1) plane of the fluorite structure.[23] Therefore, high oxygen vacancy concentration easily results in cubic → rhombohedral phase transformation. In this study, the addition of WO_3 deceases the oxygen vacancy concentration and the corresponding defect reaction is

$$W_2O_6 + 2V_O^{\bullet\bullet} \xrightarrow[AO_2]{} 2W_A^{\bullet\bullet} + 6O_O^X \quad (5)$$

In the fluorite structure, AO_2, the addition of a W_2O_6 decreases two oxygen vacancies so suppresses cubic → rhombohedral phase transformation. Moreover, W atoms tend to be surrounded by 6 oxygen atoms and form the WO_6 octahedron which limits the moving of O^{2-}.[24] It is suggested that WO_3 is an appropriate dopant to suppress cubic → rhombohedral phase transformation.

3.3. The lattice parameters of the tetragonal structure

From Table 1, the lattice parameters of the tetragonal structures decrease with x increasing for the samples $(CaO)_x(WO_3)_{0.15}(BiO_{1.5})_{0.85-x}$ of $x = 0$, 0.1, 0.2 and 0.3. Since the ionic radius of Ca^{2+} is smaller than the ionic radius of Bi^{3+}, the addition of CaO tends to reduce the lattice parameters. Moreover, the substitution of Ca^{2+} for Bi^{3+} tends to increase the oxygen vacancy concentration, and the corresponding defect reaction is:

$$CaO \xrightarrow[AO_2]{} Ca_A'' + O_O^X + V_O^{\bullet\bullet} \quad (6)$$

Addition of a CaO in fluorite-structured AO_2 may result in the increase of oxygen vacancy. Therefore, the lattice parameters

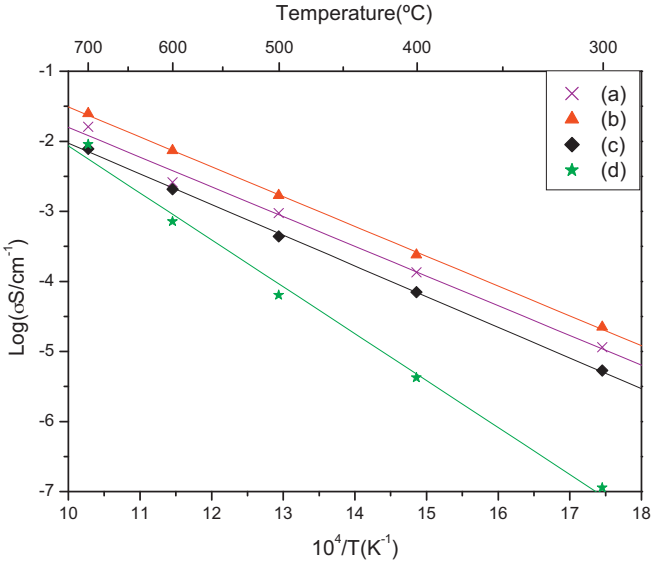

Fig. 5. Conductivities of $(Ca_xW_{0.15}Bi_{0.85-x})_2O_{3.45-x}$ for x = (a) 0, (b) 0.1, (c) 0.2 and (d) 0.3.

of the tetragonal structures decrease with x increasing for the samples $(CaO)_x(WO_3)_{0.15}(BiO_{1.5})_{0.85-x}$ of $x = 0$ and 0.1.

For the samples $(CaO)_x(WO_3)_{0.15}(BiO_{1.5})_{0.85-x}$ of $x = 0.2$ and 0.3, the compositions of the tetragonal structures are very different with those for $x = 0$ and 0.1. For the samples $(CaO)_x(WO_3)_{0.15}(BiO_{1.5})_{0.85-x}$ of $x = 0.2$ and 0.3, the compositions of the tetragonal phases were estimated to be $(CaO)_{0.173}(WO_3)_{0.119}(BiO_{1.5})_{0.708}$ and $(CaO)_{0.265}(WO_3)_{0.088}(BiO_{1.5})_{0.647}$ according to XRD results. The calculated average cation radii of $x = 0.2$ and 0.3 both are close to 1.1 Å which is larger than those (1.08 and 1.07 Å) of $x = 0$ and 0.1. However, the oxygen vacancy concentrations of $x = 0.2$ and 0.3 are 20.4% and 25% which are much higher than those of $x = 0$ and 0.1. Therefore, the lattice parameters of the tetragonal structures decrease with x increasing.

3.4. Conductivity characterization

According to Eq. (6), the substitution of Ca^{2+} for Bi^{3+} will be compensated by the creation of oxygen vacancies in order to maintain electroneutrality in the lattice. Based on these considerations, the conductivities of $(Ca_xW_{0.15}Bi_{0.85-x})_2O_{3.45-x}$ should increase with increasing content of CaO. Fig. 5 shows the conductivities of $(Ca_xW_{0.15}Bi_{0.85-x})_2O_{3.45-x}$ for x = (a) 0, (b) 0.1, (c) 0.2 and (d) 0.3. The highest conductivity is 2.35×10^{-2} S cm^{-1} at 700 °C for $x = 0.1$. For $x = 0.1$, the oxygen vacancy concentration of $(Ca_{0.1}W_{0.15}Bi_{0.75})_2O_{3.35}$ is 16.25% which is higher than 13.75% of $(W_{0.15}Bi_{0.85})_2O_{3.45}$. Therefore, the conductivity of $(Ca_{0.1}W_{0.15}Bi_{0.75})_2O_{3.35}$ is better than $(W_{0.15}Bi_{0.85})_2O_{3.45}$. For $x = 0.2$ and 0.3, the second phase $CaWO_4$ appears and blocks the oxygen conduction. Consequently, the conductivities drastically decrease and the activation energies also obvious increase for the samples $(CaO)_x(WO_3)_{0.15}(BiO_{1.5})_{0.85-x}$ of $x = 0.2$ and 0.3 as shown in Table 1.

4. Conclusion

The as-sintered $(W_{0.15}Bi_{0.85})_2O_{3.45}$ and $(Ca_{0.1}W_{0.15}Bi_{0.75})_2O_{3.35}$ exhibit a single tetragonal structure that is isostructural with $7Bi_2O_3{\cdot}2WO_3$. However, the as-sintered samples consist of a tetragonal structure and tetragonal $CaWO_4$ for $x = 0.2$ and 0.3. From the integration of XRD peak area, the compositions of matrix are $(Ca_{0.17}W_{0.11}Bi_{0.72})_2O_{3.16}$ and $(Ca_{0.24}W_{0.04}Bi_{0.72})_2O_{2.88}$ for $x = 0.2$ and 0.3, respectively. Because the oxygen vacancy concentration of matrix increases, the cubic structure is not stable for $x = 0.2$ and 0.3. Although the oxygen vacancy concentration increases with x increasing, the best conductivity is 2.35×10^{-2} S cm^{-1} at 700 °C for $x = 0.1$. $(Ca_{0.1}W_{0.15}Bi_{0.75})_2O_{3.35}$ has higher oxygen vacancy concentration (16.25%) than that of $(W_{0.15}Bi_{0.85})_2O_{3.45}$ (13.75%). Moreover, the second phase $CaWO_4$ blocks the oxygen ion mobility so $(Ca_{0.1}W_{0.15}Bi_{0.75})_2O_{3.35}$ has best conductivity among these compositions.

Acknowledgment

This work is supported by National Science Council (NSC), Taiwan, under the grant no. NSC94-2120-M-006-002.

References

1. Etsell TH, Flengas SN. Electrical properties of solid oxide electrolytes. *Chem Rev* 1970;**70**:339–76.
2. Harwig HA, Gerards AG. Electrical-properties of alpha, beta, gamma and delta phases of bismuth sesquioxide. *J Solid State Chem* 1978;**26**: 265–74.
3. Rao CNR, Subba Rao GV, Ramdas S. Phase transformations and electrical properties of bismuth sesquioxide. *J Phys Chem* 1969;**73**: 672–5.
4. Takahashi T, Iwahara H. High oxide ion conduction in sintered oxides of the system Bi_2O_3–WO_3. *J Appl Electrochem* 1973;**3**:65–72.
5. Takahashi T, Iwahara H, Esaka T. High oxide ion conduction in sintered oxide of system Bi_2O_3–M_2O_5. *J Electrochem Soc* 1977;**124**: 1563–9.
6. Takahashi T, Iwahara H. Oxide ion conductors based on bismuth sesquioxide. *Mater Res Bull* 1978;**13**:1447–53.
7. Laarif A, Theobald F. The lone pair concept and the conductivity of bismuth oxides Bi_2O_3. *Solid State Ionics* 1986;**21**:183–93.
8. Kruidhof H, Devries KJ, Burggraaf AJ. Thermochemical stability and non-stoichiometry of yttria-stabilized bismuth oxide solid-solutions. *Solid State Ionics* 1990;**37**:213–5.
9. Wachsman ED, Ball GR, Jiang N, Stevenson DA. Structural and defect studies in solid oxide electrolytes. *Solid State Ionics* 1992;**52**: 213–8.
10. Sammes NM, Gainsford GJ. Phase-stability and oxygen-ion conduction in Bi_2O_3–Pr_6O_{11}. *Solid State Ionics* 1993;**62**:179–84.
11. Azad AM, Larose S, Akbar SA. Bismuth oxide-based solid electrolytes for fuel-cells. *J Mater Sci* 1994;**29**:4135–51.
12. Shuk P, Wiemhöfer HD, Guth U, Göpel W, Greenblatt M. Oxide ion conducting solid electrolytes based on Bi_2O_3. *Solid State Ionics* 1996;**89**:179–96.
13. Watanabe A. An outline of the structure of $7Bi_2O_3{\cdot}2WO_3$ and its solid solutions. *J Solid State Chem* 1985;**60**:252–7.
14. Zhou W. Defect fluorite superstructures in the Bi_2O_3–WO_3 system. *J Solid State Chem* 1994;**108**:381–94.
15. Nespolo M, Watanabe A, Suetsugu Y. Re-investigation of the structure of $7Bi_2O_3{\cdot}2WO_3$ by single-crystal X-ray diffraction. *Cryst Res Technol* 2002;**37**:414–22.

16. Sharma N, Macquart RB, Avdeev M, Christensen M, Mclntyre GJ, Chen Y-S, et al. Re-investigation of the structure and crystal chemistry of the Bi_2O_3–W_2O_6 'type (Ib)' solid solution using single-crystal neutron and synchrotron X-ray diffraction. *Acta Crystallogr B* 2010;**B66**:165–72.
17. Abrahams I, Krok F, Chan SCM, Wrobel W, Kozanecka-Szmigiel A, Luma A, et al. Defect structure and ionic conductivity in $Bi_3Nb_{0.8}W_{0.2}O_{7.1}$. *J Solid State Electrochem* 2006;**10**:569.
18. Abrahams I, Kozanecka-Szmigiel A, Krok F, Wrobel W, Chan SCM, Dygas JR. Correlation of defect structure and ionic conductivity in delta-phase solid solutions in the Bi_3NbO_7–Bi_3YO_6 system. *Solid State Ionics* 2006;**177**:1761.
19. Hsieh CY, Fung KZ. Crystal structure and electrical conductivity of cubic fluorite-based $(YO_{1.5})_{(x)}(WO_3)_{(0.15)}(BiO_{1.5})_{(0.85-x)}$ $(0 \leq x \leq 0.4)$ solid solutions. *J Solid State Electrochem* 2009;**13**:951.
20. Shannon RD. Revised effective ionic-radii and systematic studies of interatomic distances in halides and chalcogenides. *Acta Crystallogr A* 1976;**32**:751.
21. Hsieh CY, Fung KZ. Effect of divalent dopants on defect structure and electrical properties of Bi_2WO_6. *J Phys Chem Solids* 2008;**69**:302.
22. Gellings PJ, Bouwmeester HJM. *The CRC handbook of solid state electrochemistry*. Boca Raton, FL: CRC Press; 1997. p. 82.
23. Conflant P, Boivin JC. Thermal evolution of the crystal-structure of the rhombohedral $Bi_{0.75}Sr_{0.25}O_{1.375}$ phase – a single-crystal neutron-diffraction study. *J Solid State Chem* 1994;**112**:1.
24. Islam MS, Lazure S, Vannier RN, Nowogrocki G, Mairesse G. Structural and computational studies of Bi_2WO_6 based oxygen ion conductors. *J Mater Chem* 1998;**8**:655.